SHRIMP U-PB ZIRCON GEOCHRONOLOGY OF THE DHZIDA INTRUSIVE ROCKS IN THE TAVT ORE FIELD, NORTHERN MONGOLIA

Sodnom Oyungerel[1,2*], Insung Lee[2], Luvsanchultem Jargal[1],
Batsuren Tegshbayar[3], Otgonsuren Maibayar[1,4]

[1] *School of Arts and Sciences, National University of Mongolia, Ulaanbaatar P.O.Box 46-337 Mongolia*
[2] *School of Earth and Environmental Sciences, Seoul National University, Seoul 151-747, Republic of Korea*
[3] *Jasco LLC, Ulaanbaatar, Mongolia*
[4] *Usukh gol LLC Ulaanbaatar, Mongolia*

ABSTRACT

The Tavt ore field is located in the northern part of Mongolia. The ore field containing the Tavt gold deposit, which covers 90 square km, is in the Dzhida terrane at the junction of two regional faults that trend NW and NE, respectively. This terrane, which spans the border between Mongolia and Russia is overlapped and stitched with Orkhon-Selenge trough assemblages. The geology of the deposit consists of the Early Paleozoic Dzhida intrusive complex, the Middle Paleozoic Tes intrusive complex, the Late Paleozoic Selenge intrusive complex, the Early Mesozoic Orkhon complex, and the Ediacaran-Early Cambrian metavolcanic Badariingol formation, Early Cambrian silicic-terrigenous-carbonate Burgelt formation. Zircons SHRIMP U–Pb ages from the Tavt intrusive rocks are slightly different: 505.3+3.8 Ma for plagiogranites, 512.7+4.1 to 514.4+3.0 Ma for granodiorites, 506+3.4 Ma for quartzmonzodiorites, 510.1+2.9 Ma for monzodiorites and 509.8+3.7 Ma for subalkaline diorites, respectively. It indicates that the Dzhida intrusions have formed at the island arc environment since the middle Cambrian ages.

Highlights

The zircons SHRIMP U–Pb ages are slightly different: 505.3+3.8 Ma for plagiogranites, 512.7+4.1 to 514.4+3.0 Ma for granodiorites, 506+3.4 Ma for quartzmonzodiorites, 510.1+2.9 Ma for monzodiorites and 509.8+3.7 Ma for subalkaline diorites, respectively. Tavt ore field is located in the Dzhida terrane, which has formed at the island arc environment during the middle Cambrian age.

Keywords: Dzhida intrusive rocks, Zircon SHRIMP U-Pb dating, Tavt ore field, Mongolia

***Corresponding author.** Tel.: +976-8916 0830
E-mail address: soyungerel@num.edu.mn

1. Introduction

The Tavt ore field is located in the northern Mongolia that occupies in the Central Asian Orogenic Belts. Mongolia is one of the largest Phanerozoic continental growth province. Geographically, the Tavt ore field is located close to the Russian border in Bulgan aimag, 650 kilometers northwest of Ulaanbaatar, 50 kilometers west of the Erdenet mining complex (Fig.1). The ore field containing the Tavt gold deposit is in the Dzhida terrane (Badarch et al., 2002) at the junction of two regional faults that trend NW and NE, respectively. This ore field is spatially combined with a large area of the Dzhida intrusive complex (early Paleozoic) and contains more gold and sulfide-bearing quartz veins than other complexes (Tsend-Ayush and Buldakov, 1998).

In I983, the Mongolian geological mapping expedition performed a preliminary geological survey of 1:1500000. The result of this survey, they found quartz veins with mineralization of gold, silver, copper,

molybdenum. Prospecting and reserve estimation of the Tavt gold deposit was completed by the "M and Diamond" Mongolian-Russian joint company between 1995 and 1998 (Tsend-Ayush and Buldakov, 1998). This occurrence was named "Eren". Since I997, it has been named "Tavt".

Previously, detailed geochronological studies have not been performed on this particular field. The main purpose of this paper focuses on the zircon U–Pb age. Based on the focuses, we will explain the timing.

2. Geology

The Tavt ore field covers 90 square km and is in the Dzhida terrane (Badarch et al., 2002) which spans the border between Mongolia and Russia. It is also overlapped and stitched with Orkhon-Selenge trough assemblages. The Russian part of the Dzhida terrane is composed of a stratified island arc complex restricted to a narrow strip along a NW regional shear zone. The western part of the shear zone is characterized by a huge area of the plagiogranite-tonalite-diorites. The Mongolian part of the Dzhida terrane occupies a much larger area than the Russian part (Gordienko et al., 2007, S.Khorolsuren et al., 2018). Geologically, the Mongolian part of the Dzhida terrane is located among the Tuva-Mongolia microcontinent, the Hamar-Davaa terrane, and volcano-plutonic Orkhon-Selenge trough. The Tuva-Mongolian Massif microcontinent has a Precambrian metamorphic basement and a Ediacaran-Cambrian carbonate cover (Kuzmichev, 2004; Gordienko et al., 2007). The Hamar-Davaa terrane is located in the northeast of Lake Hovsgul and extends to the Russia that is composed of Precambrian gneiss, schist, amphibolite, marble and quartzite metamorphosed to granulite facies (Badarch et al., 2002; Gordienko et al., 2007). The geology of the deposit consists of the Early Paleozoic Dzhida intrusive complex, the Middle Paleozoic (D_{2-3}) Tes intrusive complex, the Late Paleozoic (P_3-T_1) Selenge intrusive complex, the Early-Mesozoic (T_3-J_1) Orkhon complex, and the Ediacaran-Early Cambrian metavolcanic Badariingol formation, Early Cambrian silicic-terrigenous-carbonate Burgelt formation (Tsend-Ayush and Buldakov, 1998, S.Khorolsuren et al., 2018) (Fig. 1).

The Tavt ore field is mainly hosted in the Early Paleozoic Dzhida intrusive complex (Tsend-Ayush and Buldakov, 1998). The Dzhida intrusive complex, which is widely distributed in the north, south, and central part of the Tavt ore field, contains more gold and sulfide-bearing quartz veins than other complexes. Two separate phases are distinguished. The first phase comprises gabbro, gabbrodiorite, and diorites (quartz diorites, subalkaline diorites, and monzodiorites) which have gradual transitions. The first phase rocks are distributed in most of the central, southwestern and the northeastern parts of the area. These rocks contain many mafic minerals which consist of amphibole-biotite, rare amphibole-pyroxene; therefore, they are black-gray, green-gray colored, medium-grain size, and sometimes weakly porphyritic structures, gneissic or massive textures. The diorites are very widely distributed among them. These rocks occur in 20 square kilometers irregular or extensional bodies. The second phase is dominated by medium grained biotite-hornblende granodiorites and plagiogranites that are light-gray, medium grained weakly gneissoid rocks. These rocks are in contact with the first phase rocks in the southwestern, central part. Their form and locations are controlled by the NW-trending and NE-trending faults. Dzhida intrusive complex's granodiorite and plagiogranites are strongly altered by

hydrothermal brine fluids, and associated with other intrusive complexes intrusive rocks.

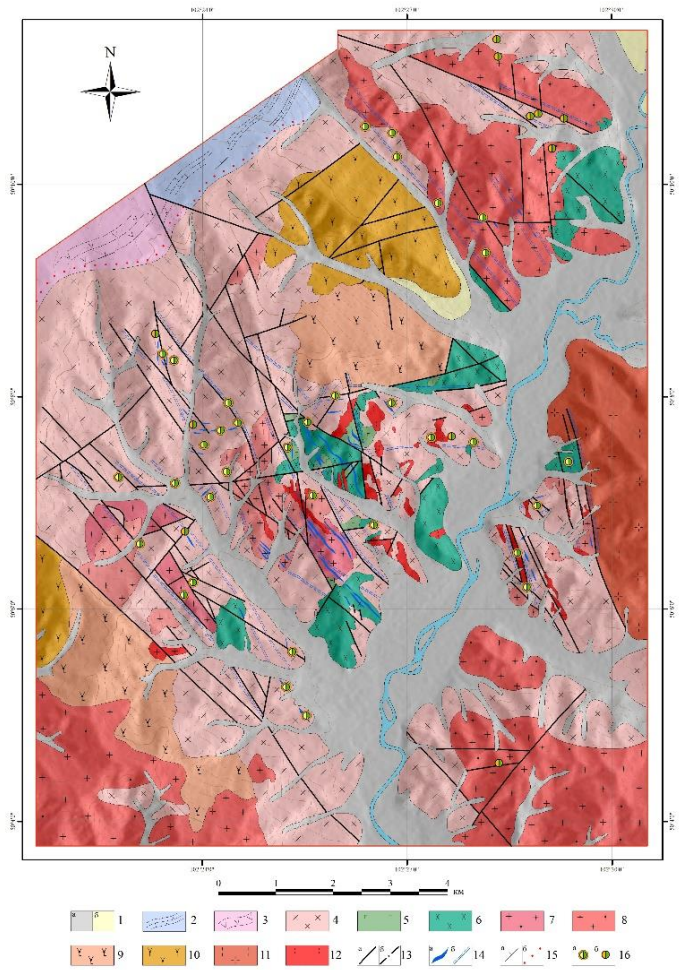

Fig. 1. Geological map of the Tavt gold deposit. 1. a-alluvial, b-colluvial; 2. Early Cambrian silicic-terrigenous-carbonate Burgelt formation; 3. Ediacaran-Early Cambrian metavolcanic Badariingol formation; Early Paleozoic: 4. granodiorite-tonalite, plagiogranite, 5. gabbro, gabbro-diorite; 6. diorites (quartz diorites, subalkaline diorites, and monzodiorites; Middle Paleozoic: 7.granites; Late Paleozoic: 8. subalkaline granites, 9. granosyenite, 10. syenite; Early Mesozoic: 11. medium–coarse grained porphyritic leucogranites, 12. fine grained aplite-like leucogranites; 13. Faults a.indicated, b.inferred; 14. a.gold-quartz veins, b.boundaries of quartz vein groups; 15.a.dip direction, b.hornfels; 16. Gold-silver-copper occurrences

3. Samples and analytical methods

3.1. Zircon sample preparation and analytical procedure for SHRIMP U-Pb dating

Six samples were collected (TV-1-14, TV-2-9, TV-3a-3, TV-3a-22, TV-40-2, and TV-2-13) from the Dzhida complex of the Tavt gold deposit field area, which is located in the northern part of Mongolia (Fig. 1). Zircons for the SHRIMP geochronology were separated from granodiorite, plagiogranite,

quartzmonzodiorite, monzodiorite and subalkaline diorite of the Early Paleozoic Dzhida intrusive complex (select a fresh, unweathered rock samples).

The rock samples were crushed with a jaw crusher and sieved. The sieved fraction was washed ultrasonically in distilled water to exclude powder residue, and then dried in an oven at 80^0C. Magnetite was removed with a hand magnet, and the magnetite free fraction was then passed through an isodynamic magnetic separator. Zircon grains were handpicked under a binocular microscope and mounted, along with pieces of the FC1 zircon standard (1099Ma, Paces and Miller, 1993), onto adhesive tape, enclosed in epoxy resin and then polished to about half their thickness.

The mount was then cleaned and gold-coated and photographed in reflected and transmitted light. The mount was photographed in backscattered (BSE) and cathodoluminescence (CL) images that are used to examine the internal structure of the analyzed zircons and with petrographic observations guided the selection of analytical spots, using a JEOL JSM-6610LV scanning electron microscope at Korea Basic Science Institute (KBSI). The U–Pb isotopic analyses were conducted using a SHRIMP IIe housed at KBSI and detailed analytical procedures are described by Willams (1998). The Squid 2.50 and Isoplot 3.71 programs were used in the ages and concordia diagrams (Ludwig, 2008, 2009).

4. Results

4.1. Zircon SHRIMP U–Pb dating

4.1.1. Granodiorite (sample TV-1-14)

Zircons from sample TV-1-14 are colorless, transparent, and subhedral to euhedral, and stubby in shape (Fig. 2a). Most are transparent and colorless, whereas a few high-uranium crystals are dark and opaque. Euhedral concentric and oscillatory zoning is common in most crystals; no inherited zircon cores were observed. They range from ~130 to 260μm in length, with length: width ratios between 1.5:1 and 2.5:1. A total of 16 spot analyses were made on 14 zircons (Fig. 3a). They have U and Th contents and Th/U ratios ranging from 37-125 ppm, 25-96 ppm and 0.65-1.03, respectively (Table 1). The best estimate of the crystallization age of sample TV-1-14, based on the weighted mean $^{206}Pb/^{238}U$ ratio is 514.4±3.0 Ma (95% confidence) (Fig. 4a).

4.1.2. Granodiorite (sample TV-2-9)

Zircon crystals in this sample are big, equant to euhedral, up to 125–325μm long, with length to width ratios of around 1.5:1 to 1.7:1(Fig. 2b). Most of the crystals are clear and colorless. In euhedral zircon crystals, concentric and oscillatory zoning is common and no inherited zircon cores are observed. A total of 22 spot analyses were made on 19 zircons (Fig. 3b). Their U and Th contents and Th/U ratios range respectively from 34-150 ppm, 26-215 ppm and 0.63-1.65 (Table 1). All 22 analyses have indistinguishable $^{206}Pb/^{238}U$ ratios within analytical error, and a weighted mean age of 512.7±4.1 (95% confidence) (Fig. 4b). This is the best estimate of the crystallization age of sample TV-2-9.

4.1.3. Plagiogranite (sample TV-3a-3)

Zircon grains in this sample are mostly big stubby or equant to euhedral, up to 140–300 μm long, with length to width ratios are 1.3:1 (Fig. 2c). Most are transparent and colorless, although a few are dark brown and turbid due to high uranium content. Euhedral concentric and oscillatory zoning is well-developed in most crystals, and no inherited zircon cores were observed. A total of 22 spot analyses was made on 19 zircon grains (Fig. 3c) and yield a weighted mean $^{206}Pb/^{238}U$ age of 505.3±3.8Ma (95% confidence) (Table 1 and Fig. 4c). The zircons have variable of Th (26-156 ppm) and

U (38-165 ppm). Th/U ratios vary between 0.62 and 1.10.

4.1.4. Monzodiorite (sample TV-3a-22)

Zircon grains were mostly clear, transparent and equant to euhedral with concentric and oscillatory zoning (Fig. 3d), up to 100–320 μm long, with length to width ratios of about 2:1 to 1.8:1 (Fig. 2d). Uranium and thorium concentrations are as follows: Th=20-76 ppm and U=31-91 ppm. Th/U ratios vary between 0.56 and 1.09 (Table 1). The eighteen analyzed spots of 16 zircon grains and yield a weighted mean $^{206}Pb/^{238}U$ age of 510.1±2.9 Ma (95% confidence interval) (Fig. 4d).

4.1.5. Quartzmonzodiorite (sample TV-40-2)

Zircon grains in this sample are euhedral, prismatic to elongate 250–450 μm long, with length to width ratios between 2:1 and 3:1 (Fig. 2e). Most are transparent and colorless, whereas a few high-uranium crystals are dark and opaque. CL imagings of most of the prismatic, elongated and fragmented larger grains have parallel bands and few grains are oscillatory zoned, although some portions are darker with less distinct zoning (Fig. 3e). The eighteen analysed spots of sixteen zircon grains from this sample were performed by SHRIMP (Table 1). Uranium and thorium concentrations are as follows: Th=20-287 ppm and U=38-251 ppm, with Th/U ratios ranging from 0.45 to 1.19. The best estimate of the crystallization age of sample TV-40-2, based on the weighted mean $^{206}Pb/^{238}U$ ratio, is 506±3.4 Ma (95% confidence) (Fig. 4e).

4.1.6. Subalkaline diorite (sample TV-2-13)

Zircon crystals in this sample are euhedral, a prism to elongate, up to 200–475 μm long, with length to width ratios of around 1.6:1 to 3.2:1 (Fig.2f). Most are clear and colorless except for few dark brown and turbid crystals. CL imaging is similar to quartzmonzodiorite (Sample TV-40-2) (Fig. 3f). These two samples (TV-40-2, TV-2-13) internal textures consistently observed in zircons from mafic and alkaline rocks (Hoskin, 2000; Yi et al., 2012). A total of 20 spot analyses were made on eighteen zircons and one of them was rejected (it has higher U, Th contents). They have variable abundances of Th (24-374ppm) and U (48-253 ppm). Th/U ratios vary between 0.43 and 1.53 (Table 1). All 19 analyses have indistinguishable $^{206}Pb/^{238}U$ ratios within analytical error and a weighted mean age of 509.8 ±3.7 Ma (95% confidence) (Fig. 4f). This is the best estimate of the crystallization age of sample TV-2-13.

The all these samples yielded Concordia ages between 505.3±3.8Ma and 514.3±4Ma, which correspond to the Middle Cambrian ($Ɛ_{2-3}$). The igneous origin zircons have Th/U>0.30 ratios (Hoskin and Schaltegger, 2003; Lang et al., 2009), the zircon SHRIMP U–Pb dating results are listed in Table 1, and related concordant diagrams are shown in Fig. 4. The TV-1-14, TV-2-9 and TV-3a-3 images on the CL have an oscillatory zone that is narrow (Fig. 3a, b and c). It directs that zircons were formed in the felsic rocks. As for the other three samples (TV-3a-22 monzodiorite, TV-40-2 quartz monzodiorite, and TV-2-13 subalkaline diorite) (Fig. 3d, e and f), the oscillatory zone is wider compared to previous three samples. Because of it, we assume that it directs the intermediate rocks. We regard that this variation of zone is similar to the pattern of plagioclase polysynthetic. Because as it becomes felsic plagioclase, the pattern of the twin becomes more narrow. On the other hand, as it becomes mafic, the pattern develops broadly.

5. Discussions

Early Paleozoic (Middle-Late Cambrian-Ordovician) magmatism manifested in the west, northwestern, north, center, southeastern part of Mongolia, as the different shapes

intrusive bodies. The intrusive rocks of Dzhida complex have been described by many Russian geologists, especially, in Russian part that recognized three phases of the Dhzida complex: gabbrodiorite, tonalite-diorite, and tonalite-plagiogranite (Distanova, 1975; Gordienko et al., 2006, 2007). The Dzhida intrusive complex occupies western and eastern fields of the Mongolian part of the Dzhida terrane. The western part of the Mongolian Dzhida terrane mainly consists of Kupchinski massif which has occurred in the Tavt ore field. Especially, it is spatially combined with a large area of the Early Paleozoic magmatism, represented by plagiogranites, granodiorite, diorites, and small intrusions of mafic rocks (gabbro, gabbrodiorites).

Zircons from the Early Paleozoic Dzhida intrusive complex indicate slightly different SHRIMP U–Pb ages: 505.3±3.8 Ma for plagiogranite, 512.7±4.1 to 514.4±3.0 Ma for granodiorites, 506±3.4 Ma for quartzmonzodiorite, 510.1±2.9 Ma for monzodiorite and 509.8±3.7 Ma for subalkaline diorite, respectively. These ages correspond to two samples from the Khotolson (quartzdiorite-504±2 Ma) and Modonhul (gabbro-506±1Ma) massifs in the Russian territory (Gordienko et al., 2007). For this reason, we suggest that the Dzhida complex intrusions were emplaced the Middle Cambrian ages ($Ɛ_{2-3}$).

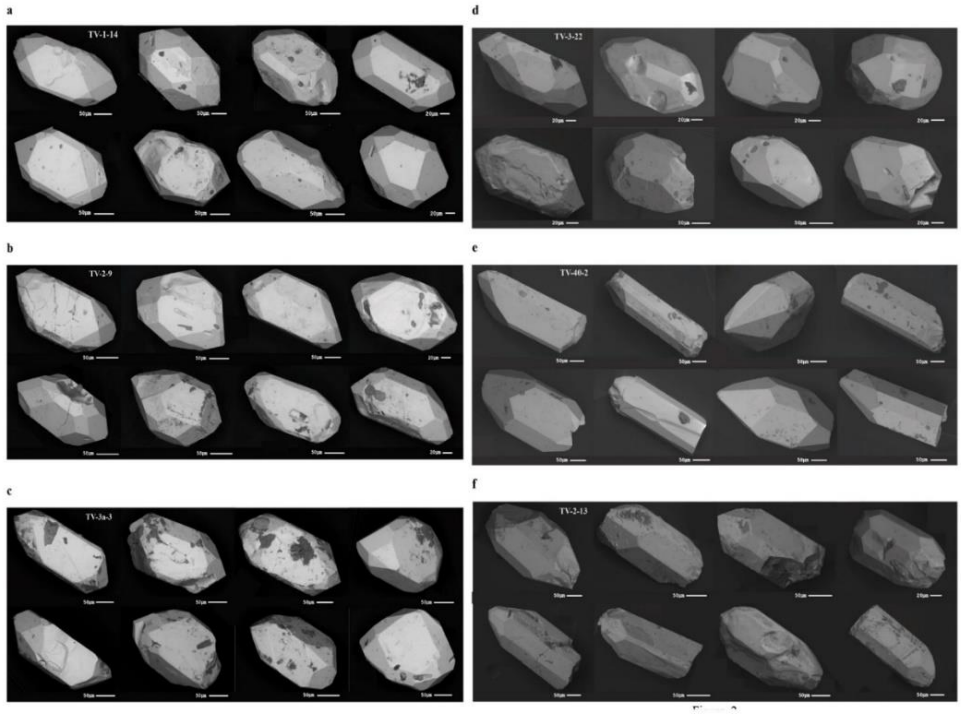

Fig. 2. SEM images of selected zircon crystals separated of Tavt ore field rocks: a-b-granodiorites; c-plagiogranite, d-monzodiorite, e-quartzmonzodiorite, f-subalkaline diorite.

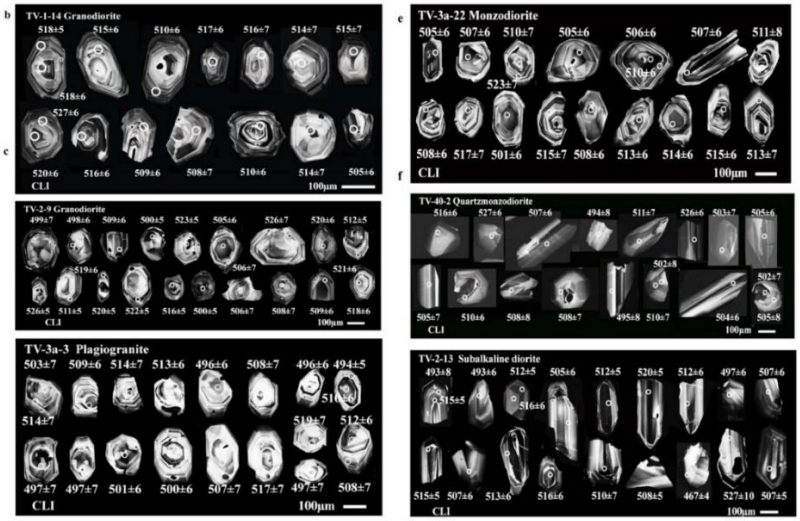

Fig. 3. Internal structures of zircon grains shown by the cathodoluminescence (CL) analysis of Tavt ore field samples: a-b-granodiorites; c-plagiogranite, d-monzodiorite, e-quartzmonzodiorite, f-subalkaline diorite.

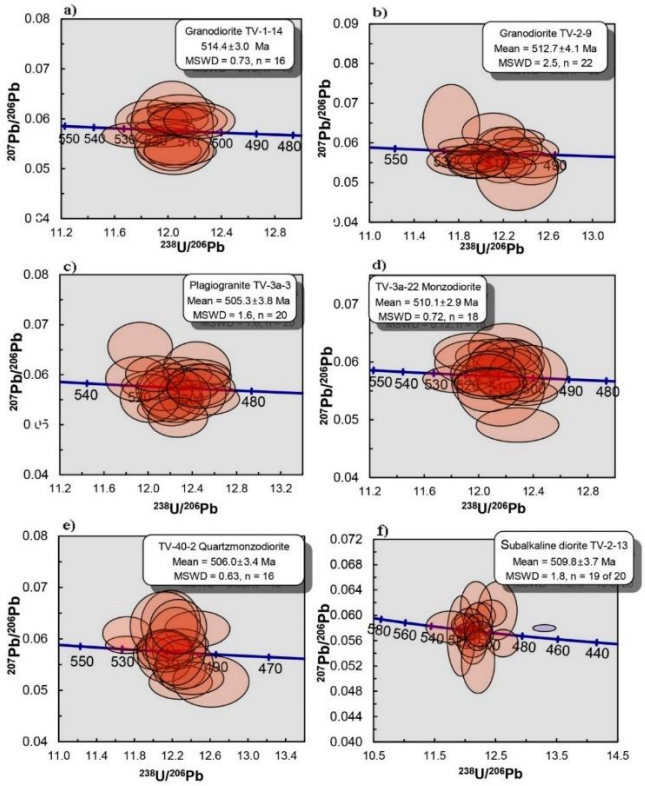

Fig. 4. Zircon SHRIMP U–Pb concordia diagrams and weighted average ^{207}Pb corrected $^{206}Pb/^{238}U$ ages of the samples from the Tavt ore field: a-b-granodiorites; c-plagiogranite, d-monzodiorite, e-quartzmonzodiorite, f-subalkaline diorite.

Table 1. Summary of SHRIMP U-Pb zircon results for 6 samples of Dzhida complex

Spot	$^{206}Pb_c$ (%)	U (ppm)	Th (ppm)	Th/U	(1) ^{238}U /$^{206}Pb^*$	±%	(1) $^{207}Pb^*$ /$^{206}Pb^*$	±%	(2) ^{206}Pb /^{238}U Age (Ma)	
TV-1-14 Granodiorite										
TV-1-14_1	0.24	125	96	0.79	12.00	1.0	0.0547	2.4	518	±5
TV-1-14_2	0.33	84	73	0.90	12.02	1.1	0.0531	3.5	518	±6
TV-1-14_3	0.51	68	48	0.72	12.10	1.2	0.0521	5.7	515	±6
TV-1-14_4	0.37	90	58	0.67	12.15	1.1	0.0565	2.8	510	±6
TV-1-14_5	0.53	75	57	0.79	11.96	1.2	0.0584	2.8	517	±6
TV-1-14_6	0.73	37	25	0.68	12.05	1.5	0.0542	8.0	516	±7
TV-1-14_7	1.24	43	28	0.67	12.21	1.5	0.0472	9.6	514	±7
TV-1-14_8	0.52	54	37	0.71	12.23	1.4	0.0445	8.3	515	±7
TV-1-14_9	0.41	67	43	0.67	11.83	1.3	0.0520	5.1	527	±6
TV-1-14_10	0.52	68	66	0.99	11.97	1.3	0.0535	4.8	520	±6
TV-1-14_11	0.15	112	63	0.58	12.13	1.1	0.0482	4.7	516	±6
TV-1-14_12	0.66	77	57	0.77	12.17	1.2	0.0577	3.3	509	±6
TV-1-14_13	1.03	46	29	0.65	12.43	1.5	0.0413	11.6	508	±7
TV-1-14_14	0.69	69	51	0.77	12.21	1.3	0.0534	4.9	510	±6
TV-1-14_15	0.94	56	56	1.03	12.10	1.3	0.0545	5.4	514	±7
TV-1-14_16	0.62	76	70	0.94	12.31	1.2	0.0552	4.0	505	±6
TV-2-9 Granodiorite										
TV-2-9_1	0.53	41	26	0.66	12.59	1.4	0.0457	8.7	499	±7
TV-2-9_2	0.28	79	73	0.96	12.45	1.1	0.0571	2.4	498	±6
TV-2-9_3	0.75	65	65	1.03	12.18	1.2	0.0573	3.7	509	±6
TV-2-9_4	0.38	145	125	0.89	12.42	1.0	0.0563	2.2	500	±5
TV-2-9_5	0.20	134	215	1.65	11.86	1.1	0.0553	2.2	523	±5
TV-2-9_6	0.77	54	55	1.06	12.37	1.3	0.0513	6.0	505	±6
TV-2-9_7	0.56	46	29	0.65	12.28	1.3	0.0554	4.6	506	±7
TV-2-9_8	0.55	44	37	0.85	11.90	1.4	0.0480	7.5	526	±7
TV-2-9_9	0.21	53	45	0.88	11.91	1.2	0.0578	2.7	520	±6
TV-2-9_10	0.20	150	135	0.93	12.12	1.0	0.0567	1.7	512	±5
TV-2-9_11	0.16	126	110	0.90	11.79	1.0	0.0565	1.9	526	±5
TV-2-9_12	0.49	55	50	0.93	11.92	1.2	0.0580	3.1	519	±6
TV-2-9_13	0.27	102	78	0.80	12.11	1.1	0.0577	2.0	511	±5
TV-2-9_14	0.20	119	96	0.83	11.90	1.0	0.0574	1.9	520	±5
TV-2-9_15	0.35	116	74	0.66	11.88	1.0	0.0572	2.1	522	±5
TV-2-9_16	0.07	126	112	0.92	12.04	1.1	0.0545	2.4	516	±5
TV-2-9_17	0.20	123	135	1.14	12.43	1.1	0.0548	2.5	500	±5
TV-2-9_18	1.42	34	29	0.90	12.30	1.5	0.0536	8.0	506	±7
TV-2-9_19	0.89	53	46	0.91	12.34	1.4	0.0476	8.9	508	±7
TV-2-9_20	1.27	46	31	0.70	12.20	1.3	0.0560	5.6	509	±6
TV-2-9_21	0.79	56	34	0.63	11.87	1.2	0.0577	3.6	521	±6
TV-2-9_22	1.17	52	48	0.96	11.90	1.3	0.0608	3.9	518	±6

Spot	$^{206}Pb_c$ (%)	U (ppm)	Th (ppm)	Th/U	(1) ^{238}U /$^{206}Pb^*$	±%	(1) $^{207}Pb^*$ /$^{206}Pb^*$	±%	(2) ^{206}Pb /^{238}U Age (Ma)	Spot
TV-3a-3 Plagiogranite										
TV-3a-3_1	1.20	38	26	0.72	12.35	1.5	0.0553	6.6	503	±7
TV-3a-3_2	0.96	51	33	0.68	12.05	1.5	0.0574	6.7	514	±7
TV-3a-3_3	0.40	70	74	1.10	12.22	1.2	0.0546	3.7	509	±6
TV-3a-3_4	0.54	49	34	0.71	12.08	1.3	0.0547	4.7	514	±7
V-3a-3_5	0.10	103	82	0.83	12.15	1.1	0.0524	3.2	513	±6
TV-3a-3_6	0.77	48	49	1.06	12.43	1.3	0.0620	2.7	496	±6
TV-3a-3_7	0.72	52	48	0.96	12.15	1.3	0.0601	5.0	508	±7
TV-3a-3_8	0.66	46	34	0.76	12.65	1.4	0.0475	7.8	496	±6
TV-3a-3_9	0.39	165	156	0.97	12.52	1.0	0.0600	1.2	494	±5
TV-3a-3_10	0.40	97	102	1.09	12.19	1.1	0.0541	3.4	510	±6
TV-3a-3_11	0.67	45	30	0.68	12.52	1.4	0.0551	5.0	497	±7
TV-3a-3_12	0.88	48	35	0.76	12.49	1.3	0.0561	6.1	497	±7
TV-3a-3_13	0.40	73	44	0.62	12.43	1.2	0.0535	3.9	501	±6
TV-3a-3_14	0.68	48	48	1.02	12.42	1.3	0.0551	5.0	500	±6
TV-3a-3_15	0.72	41	31	0.78	12.35	1.4	0.0494	7.5	507	±7
TV-3a-3_16	0.29	58	46	0.83	12.09	1.3	0.0507	7.2	517	±7
TV-3a-3_17	0.58	47	43	0.95	12.08	1.4	0.0474	7.8	519	±7
TV-3a-3_18	0.72	65	57	0.91	12.09	1.2	0.0585	3.5	512	±6
TV-3a-3_19	0.35	55	35	0.65	12.31	1.3	0.0489	7.5	508	±7
TV-3a-3_20	1.22	40	32	0.83	12.51	1.4	0.0554	6.4	497	±7
TV-3a-22 Monzodiorite										
TV-3a-22_1	0.33	83	55	0.69	12.33	1.2	0.0541	3.5	505	±6
TV-3a-22_2	0.53	72	72	1.03	12.32	1.3	0.0517	4.9	507	±6
TV-3a-22_3	0.51	41	26	0.64	12.33	1.5	0.0452	9.2	510	±7
TV-3a-22_4	0.57	57	33	0.60	11.81	1.3	0.0593	3.2	523	±7
TV-3a-22_5	0.57	71	71	1.03	12.29	1.2	0.0557	3.7	505	±6
TV-3a-22_6	0.66	72	76	1.09	12.26	1.2	0.0573	4.6	506	±6
TV-3a-22_7	0.78	56	33	0.61	12.15	1.3	0.0571	4.4	510	±6
TV-3a-22_8	0.38	91	72	0.82	12.22	1.1	0.0578	2.5	507	±6
TV-3a-22_9	1.06	31	20	0.69	12.16	1.6	0.0548	10.2	511	±8
TV-3a-22_10	0.37	78	46	0.60	12.23	1.2	0.0557	4.0	508	±6
TV-3a-22_11	1.16	51	43	0.87	12.02	1.3	0.0547	6.0	517	±7
TV-3a-22_12	0.67	58	58	1.04	12.38	1.3	0.0563	4.1	501	±6
TV-3a-22_13	1.13	37	27	0.74	12.07	1.5	0.0538	7.0	515	±7
TV-3a-22_14	0.81	65	67	1.07	12.19	1.2	0.0583	3.6	508	±6
TV-3a-22_15	0.66	58	52	0.94	12.10	1.3	0.0554	4.4	513	±6
TV-3a-22_16	0.61	77	68	0.92	12.04	1.2	0.0577	3.1	514	±6
TV-3a-22_17	0.32	88	73	0.86	12.05	1.1	0.0560	2.9	515	±6
TV-3a-22_18	0.94	49	27	0.56	12.06	1.3	0.0580	4.5	513	±7

Spot	$^{206}Pb_c$ (%)	U (ppm)	Th (ppm)	Th/U	(1) ^{238}U /$^{206}Pb^*$	±%	(1) $^{207}Pb^*$ /$^{206}Pb^*$	±%	(2) ^{206}Pb /^{238}U Age (Ma)	Spot
TV-40-2 Quartzmonzodiorite										
TV-40-2_1	0.46	109	50	0.47	12.12	1.1	0.0496	6.1	516	±6
TV-40-2_2	0.31	109	51	0.49	11.88	1.2	0.0479	5.3	527	±6
TV-40-2_3	0.98	87	67	0.80	12.32	1.3	0.0511	6.5	507	±6
TV-40-2_4	2.40	38	20	0.53	12.73	1.7	0.0449	14.9	494	±8
TV-40-2_5	0.99	76	52	0.70	12.20	1.4	0.0517	7.9	511	±7
TV-40-2_6	0.48	143	132	0.95	11.82	1.2	0.0545	3.5	526	±6
TV-40-2_7	1.35	100	57	0.59	12.49	1.4	0.0457	9.6	503	±7
TV-40-2_8	0.90	168	152	0.94	12.31	1.3	0.0552	4.1	505	±6
TV-40-2_9	1.81	99	78	0.82	12.40	1.5	0.0491	10.8	505	±7
TV-40-2_10	0.57	231	164	0.74	12.21	1.3	0.0540	4.9	510	±6
TV-40-2_11	2.01	67	52	0.80	12.32	1.7	0.0491	13.0	508	±8
TV-40-2_12	1.47	85	43	0.53	12.35	1.6	0.0477	10.6	508	±7
TV-40-2_13	2.73	54	31	0.60	12.76	1.9	0.0424	17.0	495	±8
TV-40-2_14	2.28	73	33	0.47	12.53	1.8	0.0447	14.9	502	±8
TV-40-2_15	1.21	135	99	0.76	12.16	1.6	0.0559	10.5	510	±7
TV-40-2_16	0.68	251	287	1.19	12.33	1.3	0.0552	3.0	504	±6
TV-40-2_17	1.95	98	42	0.45	12.28	1.6	0.0561	11.1	505	±8
TV-40-2_18	0.89	205	191	0.96	12.38	1.4	0.0549	6.1	502	±7
TV-2-13 Subalkaline diorite										
TV-2-13_1	1.82	101	49	0.50	12.69	1.6	0.0499	11.2	493	±8
TV-2-13_2	0.18	152	78	0.53	12.06	1.0	0.0556	2.1	515	±5
TV-2-13_3	0.84	71	46	0.66	12.64	1.2	0.0534	4.5	493	±6
TV-2-13_4	0.23	147	61	0.42	12.14	1.0	0.0553	2.2	512	±5
TV-2-13_5	0.46	90	38	0.44	12.03	1.1	0.0557	3.1	516	±6
TV-2-13_6	0.78	52	24	0.48	12.31	1.3	0.0550	4.8	505	±6
TV-2-13_7	0.10	180	191	1.09	12.13	1.0	0.0547	1.9	512	±5
TV-2-13_8	0.14	253	374	1.53	11.93	1.0	0.0562	1.4	520	±5
TV-2-13_9	0.55	62	43	0.71	12.07	1.2	0.0585	3.0	512	±6
TV-2-13_10	0.80	55	25	0.46	12.43	1.2	0.0596	3.3	497	±6
TV-2-13_11	0.55	67	43	0.67	12.24	1.2	0.0570	4.7	507	±6
TV-2-13_12	0.41	101	68	0.70	12.00	1.1	0.0591	2.0	515	±5
TV-2-13_13	0.86	71	35	0.50	12.22	1.2	0.0572	5.0	507	±6
TV-2-13_14	0.52	82	52	0.65	12.07	1.1	0.0582	2.7	513	±6
TV-2-13_15	0.26	80	46	0.60	12.04	1.1	0.0554	3.0	516	±6
TV-2-13_16	0.76	48	33	0.71	12.24	1.3	0.0503	8.7	510	±7
TV-2-13_17	0.47	202	210	1.07	12.21	1.0	0.0562	2.0	508	±5
TV-2-13_18	0.41	1753	620	0.37	13.32	0.9	0.0561	0.6	467	±4

TV-2-13_19	0.46	54	32	0.61	11.81	2.0	0.0534	4.8	527	±10
TV-2-13_20	0.33	126	95	0.78	12.24	1.1	0.0560	2.4	507	±5

Pb^{*} -radiogenic Pb.

(1) -Common Pb corrected using measured ^{204}Pb.

(2) -Common Pb corrected by assuming $^{206}Pb/^{238}U$-$^{207}Pb/^{235}U$ age concordance.

6. Conclusions

The Tavt ore field mostly hosted in the Dhizda intrusive complex that consists of wide ranges composition magmatic rocks that are associated with the Middle Paleozoic Tes intrusive complex, Late Paleozoic Selenge complex and Early Mesozoic Orkhon complex. Euhedral concentric zoning is common and no inherited zircon cores were observed, and all of the zircon Th/U ratios are bigger than 0.3, indicating it is of magmatic origin. Zircons from the Early Paleozoic Dzhida intrusive complex indicate slightly different SHRIMP U–Pb ages: 505.3+3.8 Ma for plagiogranites, 512.7+4.1 to 514.4+3.0 Ma for granodiorites, 506+3.4 Ma for quartzmonzodiorites, 510.1+2.9 Ma for monzodiorites and 509.8+3.7 Ma for subalkaline diorites, respectively.

Acknowledgements

We would like to thank SHRIMP team in KBSI for their enthusiastic help in SHRIMP-zircons U–Pb dating as well as DA He Lim and S.Khorolsuren for their shared knowledge and kindness.

Special appreciation to Mr. M.Baatar, Head of the M & Daimond Company of the Tavt gold deposit, for giving us access to the mine area to collect samples, and E.Purevsuren for his help during in field trip.

S.Oyungerel is supported by GSFS (Graduate Scholarship for Excellent Foreign Students) program and the Brain Korea 21 fund at Seoul National University. In addition, the study was financially supported by a grant from the National University of Mongolia (advanced level research grant project P2016-1111).

References

Aleinikoff, J.N., Wintsch, R.P., Fanning, C.M., Dorais, M.J., 2002. U-Pb geochronology of zircon and polygenetic titanite from the Glastonbury Complex, Connecticut, USA: in integrated SEM. EMPA, TIMS, and SHRIMP study. Chemical Geology 188, 125-147. https://doi.org/10.1016/S0009-2541(02)00076-1

Badarch, G., Cunningham, W.D., Windley, B.F., 2002. A new terrane subdivision for Mongolia: implications for the Phanerozoic crustal growth of Central Asia. J.Asian Earth Sci. 21, 87-110. https://doi.org/10.1016/S1367-9120(02)00017-2

Belousova, E.A., Griffin, W.L., O'Reilly, S.Y., 2006. Zircon crystal morphology, trace element signatures and Hf isotope composition as a Tool for Petrogenetic Modelling: Examples from eastern Australian granitoids. J. Petrology 47, 329-353. https://doi.org/10.1093/petrology/egi077

Berzina, A.P., Sotnikov, V.I., 2008. Character of formation of the Erdenet-Ovoo porphyry Cu-Mo magmatic center (Northern Mongolia) in the zone of influence of a Permo-Trassic plume. Russian Geology and Geophysics 49, 534-544.

Byamba, G., Tumorkhuu, D., Dejidmaa, G., 2011a. Tectonics lithospheric plates. Geology and Mineral Resource of Mongolia. IV (Pt 1), 93-139. ISSN: 978-99929-4-697-0: Mongolian.

Byamba, G., Dorjsuren, B., Dorjnamjaa, D., Tumorkhuu, D., Makhbadar, Ts., 2011b. Tectonics lithospheric plates. Geology and Mineral Resource of Mongolia. IV (Pt 3), 197-319. ISSN: 978-99929-4-697-0: Mongolian.

Byamba. G., 2011c. Tectonics lithospheric plates. Geology and Mineral Resource of Mongolia. IV (Pt 4), 320-394. ISSN: 978-99929-4-697-0: Mongolian.

Distanova, A.N., 1975. Early Paleozoic granitoid complex in the Dzhida area (southwestern

Transbaikalia), in Early Paleozoic granitoid complexes in western Transbaikalia and Kuznetsk Alatau, Novosibirsk. Nauka. 49–123. Russian

Gerel, O., 2011a. Geology and Mineral Resource of Mongolia: Intrusive rocks. III (Pt 1), 15-43. ISSN: 978-99929-4-653-9. Mongolian.

Gerel, O., 2011b. Geology and Mineral Resource of Mongolia: Intrusive rocks. III (Pt 6), 286-377. ISSN: 978-99929-4-653-9. Mongolian.

Glasmacher, U.A., Tschernoster. R., Clauer, N., Spaeth, G., 2001. K-Ar dating of magmatic sericite crystallites for determination of cooling paths of metamorphic overprints. Chemical Geology 175, 673-687. https://doi.org/10.1016/S0009-2541(00)00292-8

Gordienko, I.V., Kovach, V.P., Gorokhovsky, D.V., Salnikova, E.B., Kotov, A.B., Yakovleva, S.Z., 2006. Composition, U-Pb Age, and Geodynamic Setting of Island-Arc Gabbroids and Granitoids of the Dzhida Zone (*Southwestern Transbaikalia, Northern Mongolia*). Russian Geology and Geophysics 47, 956-962.

Gordienko, I.V., Filimonov, A.V., Minina, O.R., Gornova, M.A., Medvedev, A.Ya., Klimuk, V.S., et al., 2007. Dzhida island-arc system in the Paleoasian Ocean: structure and main stages of Vendian-Paleozoic geodynamic evolution. Russian Geology and Geophysics 48, 91-106.

Hendrix, M.S., Graham, S.A., Berbard, B., 1999. A review of the raletionships between granitoid types, their origins and their geodynamic environments.Lithos 46, 605-626. https://doi.org/10.1016/S0024-4937(98)00085-1

Hoskin, P.W.O., 2000. Patterns of chaos: fractal statistics and oscillatory chemistry of zircon, Geochemica et Cosmoschimica Acta 64, 1905-1923. https://doi.org/10.1016/S0016-7037(00)00330-6

Janh, B.M., Litvinovsky, B.A., Zanvilevich, A.N., Reichow, M., 2009. Peralkaline granitoid magmatism in the Mongolian-Transbaikalian Belt: Evolution, petrogenesis and tectonic significance. Lithos 13, 521-539. https://doi.org/10.1016/j.lithos.2009.06.015

Jiang, Y.H., Liao, S.Y., Yang, W.Z., Shen, W.Z., 2008, An island ars origin of plagiogranites at Oytag, western Kunlun orogen, northwest China: SHRIMP zircon U-Pb chronology, elemental and Sr-Nd-Hf isotopic geochemistry and Paleozoic tectonic implications. Lithos 106, 323-335. https://doi.org/10.1016/j.lithos.2008.08.004

Karimpour, M.H., Stern, C.R., Farmer, G.L., 2010. Zircon U-Pb geochronology, Sr-Nd isotope analyses, and petrogenetic study of the Dehnow diorite and Kuhsangi granodiorite (Paleo-Tethys), NE Iran. J.Asian Earth Sci. 37, 384-393. https://doi.org/10.1016/j.jseaes.2009.11.001

Khorolsuren, S., Azjargal,G., Udaanjargal, Kh., Tegshbayar, B., Altanzul, Ch., Enkhtuya, J., Munkhzul, G., Erdenesuvd, S., Ankhbayar, E., Urjinkhand, B., Batzorig, G., 2018. Report "Mongolian Geological Mapping 1:200 000 scale", Code-UGZ-200-T-V, Ulaanbaatar.

Kovalenko, V.I., Yarmolyuk, V.V., Kovach, V.P., Kotov, A.B., Kozakov, I.K., Salnikova, E.B., et al., 2004. Isotope provinces, mechanisms of generation and sources of the continental crust in the Central Asian mobile belt: geological and isotopic evidence. J. Asian Earth Sci. 23, 605–627. https://doi.org/10.1016/S1367-9120(03)00130-5

Kroner, A., Windley, B.F., Badarch, G., Tomurtogoo, O., Hegner, E., Jahn, B.M., et al., 2007. **Accretionary growth and crust formation in the Central Asian Orogenic Belt and comparison with the Arabian-Nubian shield.** Geological Society of America Memoirs 200, 181-209. https://doi.org/10.1130/2007.1200(11)

Kuzmichev, A., Kroner, A., Hegner, E., Dunyi, L., Yusheng, W., 2005. The Shishkhid ophiolite, northern Mongolia: A key to the reconstruction of a Neoproterozoic island-arc system in central Asia. Precambrian Research 138, 125-150. https://doi.org/10.1016/j.precamres.2005.04.002

Lee, C.A., Morton, D.M., Kistler, R.W., Baird, A.K., 2007. Petrology and tectonics of Phanerozoic continent formation: From island arcs to accretion and continental arc magmatism. Earth and Planetary Science Letters 263, 370-387. https://doi.org/10.1016/j.epsl.2007.09.025

Ludwig, K.R., 2008. User's manual for Isoplot 3.6: A Geochronological Toolkit for Microsoft Excel. Berkeley Geochronology Center Special Publication: Berkeley.

udwig, K.R., 2009. User's manual for SQUID 2. Berkeley Geochronology Center Special Publication: Berkeley.

Maniar, P.D., Piccoli, P.M., 1989. Tectonic discrimination of granitoids. Geological Society of America Bulletin 101, 635-643.

Marinov, N.A., 1973. Geology of Republic of Mongolia: Magmatism, metamorphism, and tectonic, Vol III, Moscow: Nedra; Russian

Martin-Izard, A., Fuertes-Fuente, M., Cepedal, A., Moreiras, D., Nieto, J.G., Maldonado, C., et al., 2000. The Rio Narcea gold belt intrusions: geology, petrology, geochemistry and timing. J. Geochemical Exploration 71, 103-117.

Maniar, P.D., Piccoli, P.M., 1989. Tectonic discrimination of granitoids. Geological Society of America Bulletin 101, 635-643.

Oyungerel, Sa., 2011. Geology and Mineral Resource of Mongolia: Intrusive rocks. III (Pt 5), 173-285. ISSN: 978-99929-4-653-9. Mongolian.

Oyungerel, Sod., 2002. Mineralogical study of Tavt gold deposit. Problems of geology. 222 (6), 48-52. ISSN: 99929-3-03-04. Mongolian.

Paces, J.B., Miller, J.D., 1993. Precise U-Pb ages of Duluth Complex and related mafic intrusions, Northeartern Minnesota: Geochronological insights to physical, petrogenic, paleomagnetic, and tectonomagmatic processes associated with the 1.1Ga midcontinent rift system. J. Geophysical Research-Solid Earth 98, 13997-14013.

Park, Y.S., Kim, S.W., Kee, W.S., Jeong, Y.J., Yi, K., Kim, J., 2009. Middle Jurassic tectono-magmatic evolution in the southwestern margin of the Gyeonggi Massif, South Korea. Geosciences Journal. The Association of Korea Geoscience Societies and Springer 13/3, 217-231.

Pearce, J.A., Harris, N.B.W., Tindle, A.G., 1984. Trace element discrimination diagrams for the tectonic interpretation of granitic rocks. J. Petrology 25, 956-983.

Rollinson, H.R., 1993. Using Geochemical Data: Evaluation, Presentation, Interpretation. England: Longman Group.

Sengor, A. M.C., Natal'in, B.A., Burtman, V.S., 1993. Evolution of the Altaid tectonic collage and Palaeozoic crustal growth in Eurasia. Nature 364, 299–307. doi:10.1038/364299a0

Seltman, R., Gerel, O., Kirwin, D., 2005. Geodynamics and Metallogeny of Mongolia with special emphasis on copper and gold deposits. International Association on the Genesis of Ore Deposits (IAGOD), Guidebook Series vol.11, London.

Siddoway, C.S., Fanning, C.M., 2009. Paleozoic tectonism on the East Gondwana margin: Evidence from SHRIMP U-Pb zircon geochronology of a migmatite-granite complex in West Antarctica. Tectonophysics 477, 262-277. https://doi.org/10.1016/j.tecto.2009.04.021

Steiger, R.H., Jager, E., 1977. Subcommission on geochronology: convention on the use of decay constants in geo-and cosmochronology. Earth and Planetary Science Letters 36, 359-362. https://doi.org/10.1016/0012-821X(77)90060-7

Tsend-Ayush, J., Buldakov, H.G., 1998. ("M and Daimond" Mongolian-Russian joint company). Result of the prospecting and reserve estimation of Tavt gold deposit. Report No 1.Ulaanbaatar.

Xu, H., Ma, C., Ye, K., 2007. Early cretaceous granitoids and their implications for their collapse of the Dabie orogen, eastern China: SHRIMP zircon U-Pb dating and geochemistry. Chemical Geology 240, 238-259. https://doi.org/10.1016/j.chemgeo.2007.02.018

William, M.W., 2013. Geochemistry. Department of Earth & Atmospheric Sciences Cornell University Ithaca, New York, USA.

Willams, I.S., 1998. U-Th-Pb geochronology by ion microprobe, In: McKibben MA, Shanks III WC, Ridley WL (Eds). Ap,lications of Microanalytical Techniques to Understanding Mineralizing Processes. Society of Economic Geologists, Socorro, Reviews in Economic Geology 7, 1-35.

Willams, I.S., Cho, D.L., Kim, S.W., 2009. Geochronology, and geochemical and Nd-Sr isotopic characteristics, of Triassic plutonic rocks in the Gyeonggi Massif, South Korea: Constraints on Triassic post-collisional magmatism. Lithos 107, 239-256. https://doi.org/10.1016/j.lithos.2008.10.017

Wu, C., Yang, J., Robinson, P.T., Wooden, J.L., Mazdab, F.K., Gao, Y., 2009. Geochemistry, age and tectonic significance of granitic rocks in north Altun, northwest China. Lithos 113, 423-436. https://doi.org/10.1016/j.lithos.2009.05.009

Wu, F.Y., Jahn, B.M., Wilde, S.A., Lo, C.H., Yui, T.F., Lin, Q., et al., 2003. Highly fractionated I-type granites in NE China (I): geochronology and petrogenesis. Lithos 66, 241-273. https://doi.org/10.1016/S0024-4937(02)00222-0

Wu, F.Y., Sun, D.Y., Ge, W.C., Zhang, Y.B., Grant, M.L., 2011. Wilde, A.S., Geochronology of the Phanerozoic granitoids in northeastern China. J. Asian Earth Sci. 41, 1-30. doi:10.1016/j.jseaes.2010.11.014

Yanbo, C., Jingwen, M., 2010. Age and geochemistry of granites in Gejiu area, Yunnan province, SW China: Constraints on their petrogenesis and tectonic setting. Lithos 120, 258-276. https://doi.org/10.1016/j.lithos.2010.08.013

Zhou, T., Yuan, F., Fan, Y., Zhang, D., Cooke, D., Zhao, G., 2008. Granites in the Sawuer region of the west Junggar, Xinjiang Province, China:

Geochronological and geochemical characteristics and their geodynamic significance. Lithos 106, 191-206. https://doi.org/10.1016/j.lithos.2008.06.014Zhou, J., Li, X., Geoplot: 2006. An Excel VBA program for geochemical data plotting. Computers & Geosciences 32, 554-560. DOI:10.1016/j.cageo.2005.07.005